Mon. Not. R. Astron. Soc. **000**, 000–000 (0000) Printed 30 October 2014 (MN LATEX style file v2.2)

HST/COS detection of a Ne VIII absorber towards PG 1407+265: An unambiguous tracer of collisionally ionized hot gas? ⋆

T. Hussain[1], S. Muzahid[2], A. Narayanan[3], R. Srianand[4], B. P. Wakker[5], J. C. Charlton[2], and A. Pathak[1]

[1]*Department of Physics, Tezpur University, Tezpur 784 028, India*
[2]*The Pennsylvania State University, 525 Davey Lab, University Park, State College, PA 16802, USA*
[3]*Indian Institute of Space Science & Technology, Thiruvananthapuram 695 547, India*
[4] *Inter-University Centre for Astronomy and Astrophysics, Post Bag 4, Ganeshkhind, Pune 411 007, India*
[5]*Department of Astronomy, University of Wisconsin-Madison, 475 North Charter St., Madison, WI 53706, USA*

arXiv:1410.7804v1 [astro-ph.GA] 28 Oct 2014

Accepted. Received; in original form

ABSTRACT

We report the detection of Ne VIII in a $z_{\rm abs}$ = 0.59961 absorber towards the QSO PG1407+265 ($z_{\rm em}$= 0.94). Besides Ne VIII, absorption from H I Lyman series lines (H I λ1025 – λ915), several other low (C II, N II, O II and S II), intermediate (C III, N III, N IV, O III, S IV and S V) and high (S VI, O VI and Ne VIII) ionization metal lines are detected. Disparity in the absorption line kinematics between different ions implies that the absorbing gas comprises of multiple ionization phases. The low and the intermediate ions (except S V) trace a compact ($\sim$ 410 pc), metal-rich ($Z \sim Z_{\odot}$) and over-dense ($\log n_{\rm H} \sim -2.6$) photoionized region that sustained star-formation for a prolonged period. The high ions, Ne VIII and O VI, can be explained as arising in a low density ($-5.3 \leqslant \log n_{\rm H} \leqslant -5.0$), metal-rich ($Z \gtrsim Z_{\odot}$) and diffuse ($\sim$ 180 kpc) photoionized gas. The S V, S VI and C IV (detected in the FOS spectrum) require an intermediate photoionization phase with $-4.2 < \log n_{\rm H} < -3.5$. Alternatively, a pure collisional ionization model, as used to explain the previous known Ne VIII absorbers, with $5.65 < \log T < 5.72$, can reproduce the S VI, O VI and Ne VIII column densities simultaneously in a single phase. However, even such models require an intermediate phase to reproduce any observable S V and/or C IV. Therefore, we conclude that when multiple phases are present, the presence of Ne VIII is not necessarily an unambiguous indication of collisionally ionized hot gas.

Key words: galaxies:formation – galaxies:halos – quasars:absorption lines – quasar:individual (PG 1407+265)

1 INTRODUCTION

The census of baryons at low redshift has revealed that the formation of galaxies and galaxy clusters has been a relatively slow process (Persic & Salucci 1992; Fukugita & Peebles 2004). Nearly 90% of the total number of baryons in the present universe are outside of galaxies, in circumgalactic gas and in the more distant intergalactic medium (IGM). A significant fraction ($\sim$ 30 – 50%) of these baryons are predicted to have temperatures of $T \sim 10^5 - 10^7$ K, resulting from shocks during gravitational collapse leading to structure formation (Cen & Ostriker 1999; Davé et al. 2001). This warm-hot phase of the intergalactic medium (WHIM) and the associated halo gas is a common outcome of structure formation simulations in a ΛCDM dominated universe. Observations of this diffuse gas phase are crucial for forging a full understanding of the physical and ionization conditions of matter in the universe as well for a full accounting of baryons in the present universe.

Lyα forest surveys at low-z have shown that the diffuse cool ($T \sim 10^4$ K) photoionized gas outside of galaxies contains about 30% of the total baryons (Penton et al. 2004; Lehner et al. 2007). Compared to this cooler gas phase, detections of the warm-hot gas have been scarce. At temperatures of $T \geq 10^5$ K, the neutral fraction of hydrogen is expected to be

⋆ Based on observations made with the NASA/ESA *Hubble Space Telescope*, obtained from the data archive at the Space Telescope Science Institute, which is operated by the Association of Universities for Research in Astronomy, Inc., under NASA contract NAS 5-26555.

very low $f_{\rm H\,I} \equiv N({\rm H\,I})/N_{\rm H} \leq 10^{-6}$ from collisional ionization (Sutherland & Dopita 1993). The warm-hot gas seen in Lyα will therefore be shallow and thermally broad ($b({\rm H\,I}) > 40$ km s^{-1}, see e.g. Tripp et al. 2001). Searching for these broad-Lyα absorbers (BLAs) is a proven strategy for probing warm-hot baryons and it has been shown that they have a cosmic density of $\Omega_b({\rm BLA}) \sim$ 7% (Richter et al. 2004; Sembach et al. 2004; Richter et al. 2006; Lehner et al. 2007).

An alternate means of detecting the warm-hot gas phase is to search for highly ionized metal line transitions. Among the suite of available lines, the Ne VIII $\lambda\lambda$770, 780 Å doublet is a very sensitive probe of collisionally ionized gas at $T \geq 10^5$ K. The detection of Ne VIII, often associated with O VI, has yielded physical conditions in several warm-hot absorbers (Savage et al. 2005; Narayanan et al. 2009; Savage et al. 2011; Narayanan et al. 2011; Tripp et al. 2011; Narayanan et al. 2012; Meiring et al. 2013; Tepper-García et al. 2013). Except for the first (i.e., Savage et al. 2005), eight of Ne VIII detections have come from the high sensitivity high signal-to-noise (SNR) *Hubble Space Telescope*(HST)/Cosmic Origins Spectrograph (COS) spectra in the far-ultraviolet (FUV). In all these studies Ne VIII is shown to be collisionally ionized. However, in an optically thin gas exposed to the extragalactic ionizing background radiation (Haardt & Madau 2001), the ionization fraction of Ne VIII can become considerable (i.e., $\geq$ 0.1, see e.g., Figure 1 of Tepper-García et al. 2013) under two conditions: (a) low-temperature, extremely tenuous photoionized gas (with $n_{\rm H} < 10^{-5}$ cm^{-3} and $T < 10^5$ K) and (b) warm-hot collisionally ionized gas (with $n_{\rm H} > 10^{-5}$ cm^{-3} and $T > 3 \times 10^5$ K). Therefore, the possibility that the Ne VIII originates from photoionization cannot be ruled out provided the inferred cloud sizes are not unreasonably large (see e.g., Savage et al. 2005; Narayanan et al. 2012).

Significant progress has been achieved in our understanding of the global properties of low-z O VI absorbers, another candidate for probing baryons at the lower temperature end of the $10^5 - 10^7$ K gas (Danforth et al. 2006; Tripp et al. 2008; Savage et al. 2014). From nearly 60 O VI systems currently known at $z < 0.5$, it is estimated that O VI absorbers accounts for $\leq 4 - 10$% of the total baryons, comparable to the baryon fraction trapped within galaxies (Tripp et al. 2000; Savage et al. 2002; Danforth & Shull 2005; Savage et al. 2014). The steep power-law column density distribution of the O VI absorbers suggests that the baryon fraction is likely to be more than doubled if one could detect weak ($N({\rm O\,VI}) \leqslant 10^{13.0}$ cm^{-2}) O VI systems from higher SNR data. There is a lingering concern however on the process that regulates the production of O VI in intervening absorbers. In many cases, the O VI and associated H I are consistent with an origin in collisionally ionized warm $T \sim 10^5$ K gas (Danforth & Shull 2008). But in a significantly large number of cases formation of O VI through photoionization cannot also be ruled out (Thom & Chen 2008; Tripp et al. 2008; Howk et al. 2009; Muzahid et al. 2012a; Muzahid 2014). Only the former would contribute towards the accounting of warm-hot baryons since photoionization temperatures are at least an order of magnitude lower. Ne VIII is thought to be free from such ambiguities on the gas phase it traces. However, the current sample of Ne VIII systems is insufficient. As we wait for the number of Ne VIII systems to grow, it is worthwhile analyzing suitable individual absorption systems to gain insights into the chemical, ionization conditions and the physical origin of these absorbers. In that spirit, we report a new detection and analysis of a Ne VIII absorber at $z_{\rm abs} \sim 0.6$ in the high SNR HST/COS spectrum of the quasar PG 1407+265. Previous HST observations of the quasar PG 1407+265 were reported by McDowell et al. (1995) where they discussed the unusual emission line properties of this radio-quiet quasar. HST/FOS observations of the same quasar were reported by Jannuzi et al. (1998).

This article is organized as follows: In Section 2 we describe the observation and data reduction. Detailed description of the absorbing system and measurements of individual lines are given in Section 3. Different possible ionization scenarios are explored in Section 4. In Section 5 we discuss our results and summarize the conclusions. Throughout this article, we adopt an H_0 = 70 km s^{-1}Mpc^{-1}, $\Omega_{\rm M}$ = 0.3, and Ω_Λ = 0.7 cosmology. The solar relative abundances for the heavy elements are taken from Grevesse et al. (2010).

2 OBSERVATIONS AND DATA REDUCTION

The medium resolution (i.e., $\lambda/\Delta\lambda \sim$ 18,000), high SNR (e.g., $\sim$ 40 per resolution element) FUV spectrum of PG 1407+265 ($z_{\rm em}$ = 0.94) was obtained using HST/COS during observation cycle-17 under program ID: 11741 (PI: Todd Tripp). The observations consist of G130M and G160M FUV grating integrations covering the wavelength range 1150 – 1800 Å. The properties of COS and its in-flight operations can be found in Osterman et al. (2011) and Green et al. (2012). It is now well known that the COS wavelength calibration maybe inaccurate at a level of about $\sim$ 20 km s^{-1} (Savage et al. 2011; Meiring et al. 2013). For different exposures of the same target, taken at different times and/or with different central wavelength settings, there may be offsets of up to one resolution element ($\sim$ 17 km s^{-1}) between corresponding individual spectra. One of us (BPW) has developed an algorithm to correct for this, which will be fully described elsewhere (Wakker et al. 2014 , in preparation). Briefly, this method involves cross-correlating strong non-black absorption lines produced by the Galactic interstellar medium (ISM) or intergalactic gas between exposures. This gives the relative offsets needed to align the spectra at the wavelength of the absorption line. The offsets as a function of wavelength are fitted by a polynomial. This fit is used to bring different exposures into alignment before co-addition. Finally, the ISM absorption line velocities in the co-added exposures are aligned with the corresponding 21-cm H I emission profile to get a correct absolute wavelength scale.

In Fig. 1 we show the resulting offsets for PG1407+265. Clearly, for some combinations of grating central wavelength and fixed-pattern-position (FP-POS) settings there are large differential offsets from short to long wavelengths. For example, in panel 4, the spectrum obtained with grating settings of λ(cen)=1309 Å and FP-POS=1 is plotted against the λ(cen)=1327 Å, FP-POS=4 exposure. At 1200 Å, aligning the two spectra requires shifting the λ(cen) = 1327 Å by $-$10 km s^{-1}, while at 1300 Å the shift needed is +10 km s^{-1}. Applying a constant shift across the spectrum would result in smearing out the lines in the combined spectrum. This differential shift is corrected for in the algorithm that we have used.

The reduced co-added spectra were binned by three pixels, as the COS data in general are highly oversampled (six raw pixels per resolution element). All measurements and analysis presented in this work were performed on the binned data. While binning improves the SNR (per pixel) of the data, measurements are found to be fairly independent of binning. Continuum normalization was done by fitting the line-free regions with a smooth lower-order polynomial.

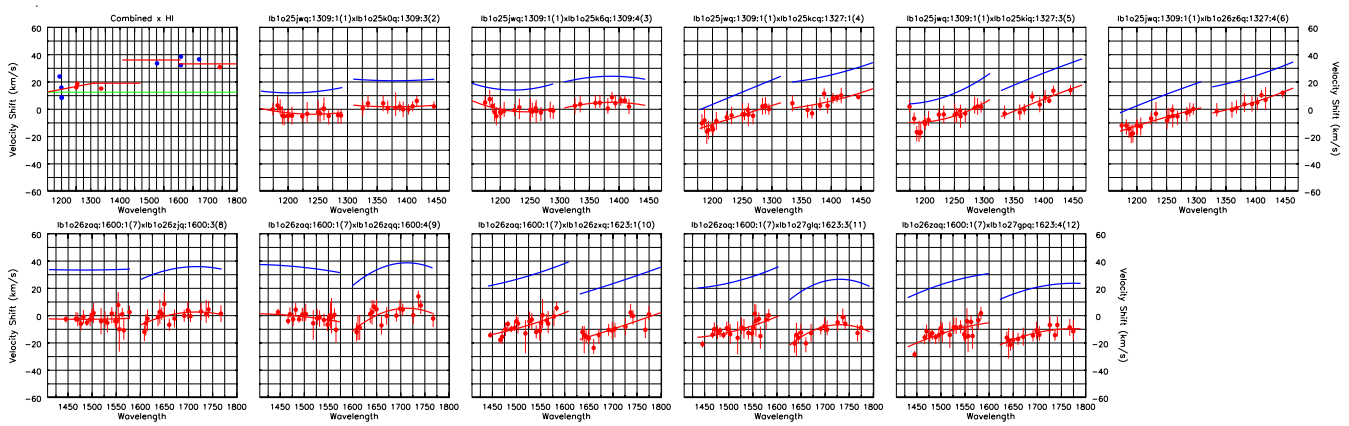

Figure 1. The first panel shows the offsets between 21-cm data and the combined, aligned spectra, while the remaining panels give the offsets needed to bring the spectra into alignment. Red points show the offset between individual absorption lines in each pair of spectra, as labeled above each panel. Only the offsets between the reference spectrum (lb1o04eoq) and the other exposures are shown. The red lines give the linear fits to these offsets. The blue lines show the combined effect of relative and absolute (w.r.t 21-cm) offsets, i.e., they show the offsets that are actually to be applied to each spectrum in order to align it with the other spectra and with the 21-cm data

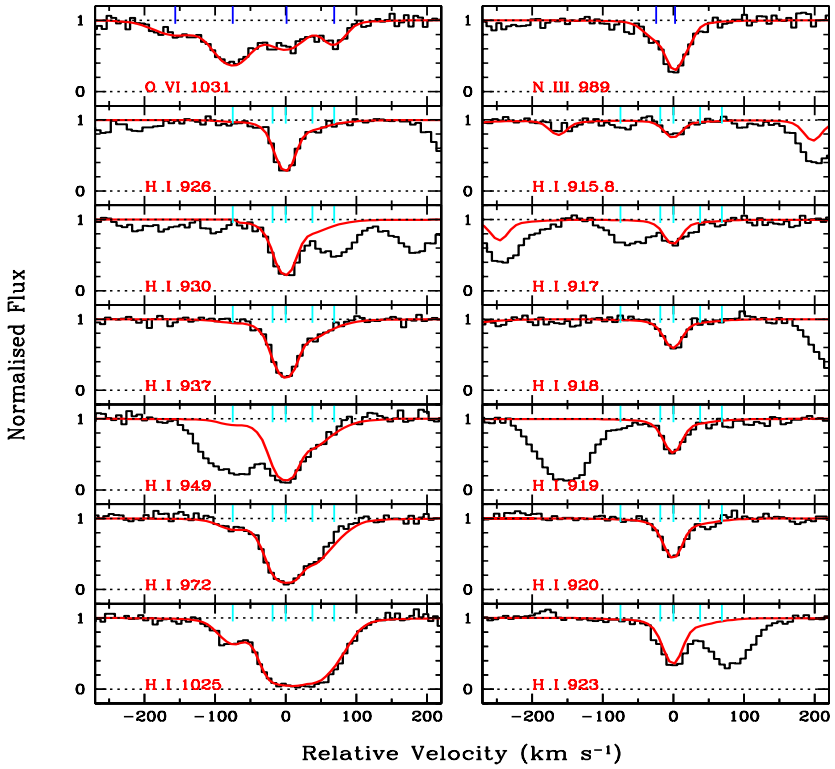

Figure 2. Continuum-normalized velocity plot for the H I Lyman series lines. Zero velocity corresponds to $z_{\rm abs}$ = 0.59961. The best fitting Voigt profiles (smooth red curves) are overplotted on top of the data (black histograms). The vertical tick marks (in cyan) represent velocity centroids of five H I components used for fitting. In the top panels, O VI (in the left) and N III (in the right) profiles are shown for comparison. While N III closely follows the component structure seen in the core of the H I absorption, the O VI profile looks very different suggesting an entirely different origin.

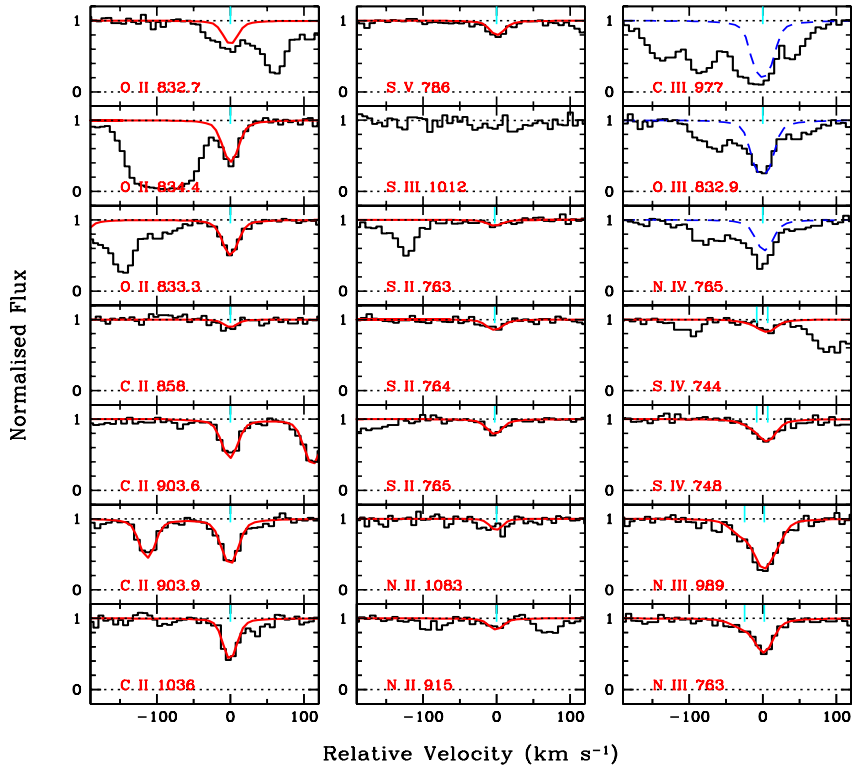

Figure 3. Continuum-normalized velocity plot for the low-ions. Zero velocity corresponds to $z_{\rm abs}$= 0.59961. The best fitting Voigt profiles are shown in smooth (red) curves on top of the data (black histogram). The vertical tick marks represent velocity centroid for each components. S III is a non-detection. Note that for N IV, O III, and C III the dashed smoothed curves are the synthetic profiles with photoionization model predicted column densities (see text).

3 SYSTEM DESCRIPTION AND LINE MEASUREMENTS

In this work we focus on the system with total N(H I) = $10^{16.03\pm0.03}$ cm^{-2} at $z_{\rm abs}$= 0.59961 that also shows Ne VIII absorption in the COS spectrum of PG 1407+265. For this system we detect absorption from H I Lyman series lines, O II, O III, O VI, C II, C III, N II, N III, N IV, S II, S III, S IV, S V, and S VI. The metal lines used in our analysis are all detected at a $> 3\sigma$ level. Continuum normalized plots of H I and prominent metal lines are shown in Fig. 2, 3, and 4. To extract the component structure, column densities and Doppler widths we applied Voigt profile fits to the lines using the VPFIT(v10.0) software package[1]. We adopt the Kriss (2011) line spread function (LSF) to take care of the non-Gaussian nature of the COS LSF. The results of these fits are summarized in Tables 1 and 2.

The hydrogen absorption associated with this absorber is detected in the Lyman series lines from H I λ1025 to λ915. Lyα is outside the wavelength coverage of the COS spectrum. Although Lyα range is covered in the FOS spectrum available in the HST archive, spectral resolution is not high enough to give additional useful information. The higher order Lyman lines are unsaturated, providing constraints on the component structure and column densities of H I. A free simultaneous fit to the Lyman lines results in a five component kinematic structure listed in Table 1 and shown in Fig. 2. The bulk of the neutral hydrogen absorption is at $v_{\rm rel}$ = 0 km s^{-1}, defined with respect to the reference redshift $z_{\rm abs}$ = 0.59961, which coincides with the single narrow component absorption seen in the low and intermediate ions. Apart from S VI, O VI, and Ne VIII, all other ions (having lower ionization energies) detected in this system are taken here to be low/intermediate ions.

The total N(H I) measured in this system is consistent with the absorber being optically thin to hydrogen ionizing photons. Therefore, the presence of singly ionized species like C II, O II, N II etc., despite the lack of shielding of ionizing radiation by H I, makes this system interesting. The presence of C II is confirmed by the detection of λ858, λ903.6, λ903.9 and λ1036 lines. The column density and b-parameter of C II were estimated by simultaneously free fitting these four lines with a single component. The O II ion transitions are seen at λ832.7, λ833 and λ834. However, the O II λ832.7 line is blended and is excluded from profile fitting.

The N II λ915 and λ1083 are very weak, but detected at a $\gtrsim 3\sigma$ level. The column density and b-value for N II were derived by keeping b and $v_{\rm rel}$ of the single component tied to the more reliable C II fit parameters. Weak absorption from S II is seen through the triplet absorption at $\lambda\lambda\lambda$ 763, 764, 765. The line parameters are derived from simultaneous fits to the three lines.

At the wavelength of N III 989 we also expect to see Si II λ989, a weaker line of Si II. The equivalent width ratio between N III λ989 and N III λ763 is $\sim 2:1$. The profiles of the two lines are also consistent with each other. Using [Si/S] solar abundance ratio and measured $\log N$(S II) = 12.53 ± 0.03, the predicted column density of Si II 989 is $\log N$(Si II) = 11.78 ± 0.03. This column density is too low to produce any detectable absorp-

[1] http://www.ast.cam.ac.uk/ rfc/vpfit.html

Table 1. Voigt profile fit parameters for H I and low ions.

Species	$v^a_{\rm rel}$	b (km s^{-1})	log N (cm^{-2})
H I	-75 ± 0	23±4	14.00±0.05
H I	-19 ± 0	18±2	14.61±0.07
H I	0 ± 0	12±1	15.97±0.02
H I	37 ± 3	22±6	14.77±0.10
H I	68 ± 0	26±5	14.26±0.10
C II	0 ± 1	7±1	14.04±0.07
O II	0 ± 1	8±1	14.14±0.03
N II	0 ± 0	7±0	13.16±0.11
N III	-25 ± 16	19±17	13.55±0.41
N III	2 ± 2	10±2	14.20±0.09
S II	-3 ± 1	9±2	12.53±0.03
S III			<13.5
S IV	-9 ± 12	19±0	12.70±0.35
S IV	7 ± 3	10±0	13.08±0.15
S V	-1 ± 1	8±2	12.41±0.03
Si II			<13.2

Note – $^a v_{\rm rel}$ is the relative velocity measured w.r.t $z_{\rm abs}$ = 0.59961.

tion. Also, a 3σ equivalent width of Si II 989 is $W = 3$ mÅ. From this, we infer the contribution from Si II at λ989 to be negligible.

The asymmetry in profile shapes of the two N III lines is indicative of unresolved multiple components contributing to the absorption. A simultaneous formal fit to the N III λ989 and λ763 does reveal two components; a weaker component at $v_{\rm rel}\sim -25$ km s^{-1} and a stronger component at $v_{\rm rel}\sim 2$ km s^{-1}. The component at $v_{\rm rel}\sim 2$ km s^{-1} has z and b consistent with those of C II & O II and contains $\sim$ 80% of the total N(N III).

C III λ977, O III λ832.9 and N IV λ765 lines are severely contaminated by absorption unrelated to the system. In Fig. 3 we show the synthetic profiles of these lines using the photoionization model predicted column densities (listed in Table 3) and assuming b(C III) = b(C II), b(O III) = b(O II), and b(N IV) = b(N III). The asymmetry in the S IV λ744 and λ748 doublet requires a two component fit, whereas a single component fit was found adequate for S V λ786. For the cases of non-detections of S III λ1012 and Si II λ889 lines, we estimate 3σ upper limits on column densities from the observed error spectrum assuming a Doppler parameter of $b = 8$ km s^{-1}.

The O VI is detected in both the $\lambda\lambda$1031, 1037 lines of the doublet. Compared to the narrow range in velocity (Δv_{90} [2] $\lesssim$ 90 km s^{-1}) over which the low ionization absorption is seen, the O VI is spread over a velocity range of $\Delta v_{90} \sim 270$ km s^{-1}. A simultaneous fit to the doublet yields four components at $v_{\rm rel}$= -157, -75, 0, and 68 km s^{-1} with respect to the reference redshift $z_{\rm abs}$ = 0.59961 (see Fig. 4). The $v = 68$ km s^{-1} component of O VI λ1037 is blended with absorption unrelated to the system, evident by comparing its strength with the corresponding component in O VI λ1032 feature.

The Ne VIII λ770 line is blended with the H I λ949 ($z_{\rm abs}$= 0.29741) and H I λ1215 ($z_{\rm abs}$= 0.01343) absorption. The Ne VIII λ780 line is however clearly detected with an observed equivalent width of $W_{\rm obs}$ = 52.84±6.55 mÅ. The Ne VIII absorption shows similar kinematic spread and velocity structure as O VI (see Fig. 4). A free fit to the Ne VIII λ780 feature results in four components with a total column density of log N (cm^{-2}) = 14.15±0.18. Voigt profile fitting results for the high ions are summarized in Table 2. It is important to note that the line centroids of Ne VIII components are consistent within 1σ of the line centroids of O VI. This strongly suggests that they originate from the same phase of the absorbing gas. A weak S VI λ933 absorption feature is detected at a 3σ level (with $W_{\rm obs}$ = 26.35±7.85 mÅ) in the two highest column density Ne VIII components. Like Ne VIII and O VI, S VI does not show any resemblance to the component structure of low ions.

[2] see Muzahid et al. (2012a) for definition.

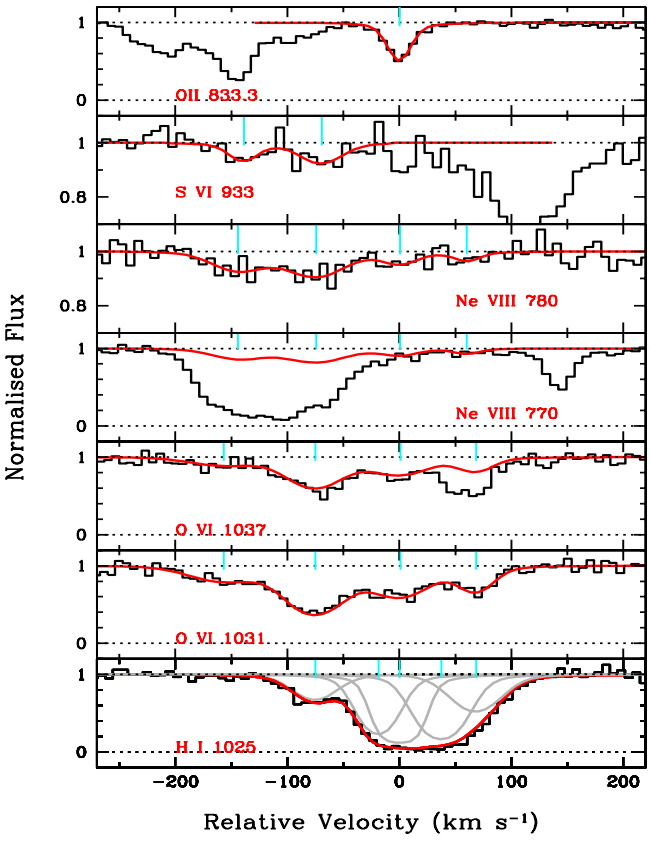

Figure 4. Same as Fig. 3 but for the high ions. In the bottom panel, individual components of H I λ1025 absorption are shown in grey curves. No Lyβ absorption is detected corresponding to the high ionization component at -150 km s^{-1}. The other three high ionization components are seen to coincide with H I. However, H I b-parameters in these components are narrower compared to O VI, suggest that they do not trace each other. In the top panel the O II profile is plotted to show the difference in kinematics of high and low ions.

In Fig. 5 we show apparent column density profiles (Savage & Sembach 1991) of several high and low ionization absorption lines detected in this system. The profiles of H I λ918, C II λ1036, and N III λ989 look remarkably similar and aligned with each other. High ionization species (S VI, O VI, and Ne VIII), on the other hand, show a completely different profile compared to C II λ1036, but follow each other. This clearly suggests multiphase nature of the absorbing gas.

4 IONIZATION MODELLING

To understand the physical conditions and the chemical enrichment in this absorber, we explore different possible ionization scenarios.

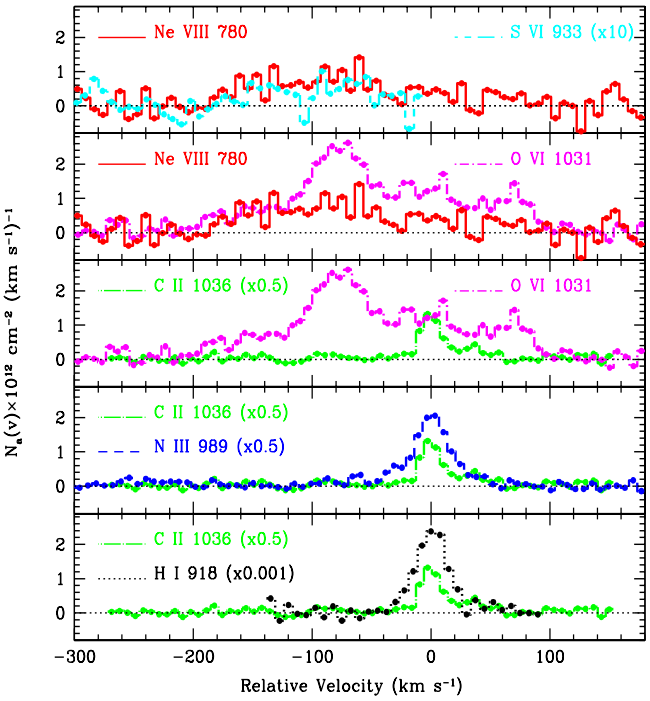

Figure 5. Apparent column density profiles (in units of 10^{12} cm^{-2} (km s^{-1})$^{-1}$) for different lines detected in this system are plotted in velocity scale. Zero velocity corresponds to $z_{\rm abs}$ = 0.59961. High and low ionization species show markedly different line kinematics.

Under the initial assumption that the gas is purely photoionized, we generate photoionization models for a range of plausible ionization parameter defined as $U = n_\gamma/n_{\rm H}$, the ratio of ionizing photon number density (n_γ) to the total hydrogen number density ($n_{\rm H}$). Grids of photoionization (PI) models were generated using CLOUDY (v13.03, last described by Ferland et al. 2013) assuming the absorbing clouds to be plane-parallel slabs with constant density having solar relative elemental abundances. The clouds were irradiated with the extragalactic UV background modelled by Haardt & Madau (2001) at z = 0.6[3]. Later on, we also investigate collisional ionization equilibrium (CIE) and constant temperature photoionization (PI+CIE) or hybrid models in order to understand the highly ionized gas phase traced by S VI, O VI, and Ne VIII.

4.1 Photoionization model

The results from photoionization models for $\log\ N({\rm H\,I}) = 15.97$ and solar metallicity are shown in Fig. 6. The H I column density is what we measure for the core absorption which coincides in velocity with the single component absorption in the low ions and also the stronger narrow component in the intermediate ions. This component has 88% of the total $N({\rm H\,I})$ measured in this system. The best constraint on the ionization parameter comes from $\log[N({\rm N\,II})/N({\rm N\,III})] = -1.04 \pm 0.14$. The models are consistent with this observed column density ratio in the interval

[3] An updated version of the extragalactic UV background is presented by Haardt & Madau (2012). We find that our conclusions remain unchanged when we use this updated background radiation.

Table 2. Voigt profile fit parameters for Ne VIII, O VI, and S VI.

Ion	$v_{\rm rel}$ (km s^{-1})	b(km s^{-1})	$\log N$ (cm^{-2})
Ne VIII	-144 ± 11	29±16	13.65±0.19
O VI	-157 ± 7	38±11	13.67±0.09
S VI	-139 ± 6	14±10	12.39±0.14
Ne VIII	-74 ± 8	31±15	13.80±0.15
O VI	-75 ± 2	30± 3	14.26±0.03
S VI	-69 ± 7	22±10	12.58±0.11
Ne VIII	0 ± 9	18±17	13.30±0.22
O VI	0 ± 3	31± 6	13.96±0.06
Ne VIII	60 ± 10	11±19	13.08±0.27
O VI	68 ± 2	18± 4	13.69±0.06

$-2.7 \leqslant \log U \leqslant -2.5$, which corresponds to a density range of $n_{\rm H} = (2-3) \times 10^{-3}$ cm^{-3} (the shaded region in Fig. 6). As the gas is optically thin to H I ionizing photons, this density range is not sensitive to the $N({\rm H\,I})$ value we assumed in the model. The best fit model for low and intermediate ions is obtained for $\log U \sim -2.6$. This corresponds to a density of $n_{\rm H} = 2.5 \times 10^{-3}$ cm^{-3}, total hydrogen column density of $\log N_{\rm H}$ (cm^{-2}) = 18.5, and line-of-sight thickness of $\sim$ 410 pc. The density we infer here is larger than the inferred $n_{\rm H}$ in the cool (or low ionization) phase of the other known Ne VIII absorbers (see Table 1 of Tepper-García et al. 2013). The photoionization equilibrium temperature, as predicted by CLOUDY, is $T \sim 10^{3.9}$ K. The measured Doppler parameter in the strongest H I component, $b({\rm H\,I}) = 12 \pm 1$ km s^{-1} (see Table 1), is consistent with this temperature.

In Table 3 we present a comparison of observed and model predicted ionic column densities for different species. The model predicted values are calculated at $\log n_{\rm H} = -2.6$, $\log Z/Z_\odot = 0$, and $\log N({\rm H\,I})$ = 15.97. Column 4 of the table gives the corrections to the elemental abundances that are required to match the observed column densities. It is clear that within 0.2 dex, the relative abundances of C, N, O and S are consistent with a solar abundance pattern. Absolute metallicity close to solar with solar relative abundances is consistent with the absorbing gas originating from a region having a chemical history similar to the Galactic ISM at the epoch of the formation of the Sun. Note that the [N/O] = 0.01 ± 0.11 is close to solar in this system. It is well known that nitrogen can be produced either by a primary or secondary route depending on whether the seeds (carbon and oxygen) were produced in the star during the helium burning stage or were already present in the star. Primary N is synthesized from intermediate mass stars on the asymptotic giant branch (AGB) while secondary N is produced most effectively by all hydrogen burning stars. It has been observed that for oxygen abundance [O/H] $\gtrsim -0.4$, the [N/O] ratio rises with increasing [O/H] (secondary N). However at lower metallicities (e.g., [O/H] $\lesssim -0.7$), the [N/O] ratio remain constant at -0.5 (primary N). The measured high value of [N/O] along with the solar metallicity suggests that nitrogen in this system is predominantly produced via the secondary route. Therefore the absorbing gas was possibly a part of a region that sustained star-formation for a prolonged period. The chemical enrichment in this absorber is unlike what is seen in the high redshift DLAs (Petitjean et al. 2008; Cooke et al. 2011; Dutta et al. 2014) but it corresponds to what we see in the interstellar medium (ISM) of our Galaxy (Israelian et al.

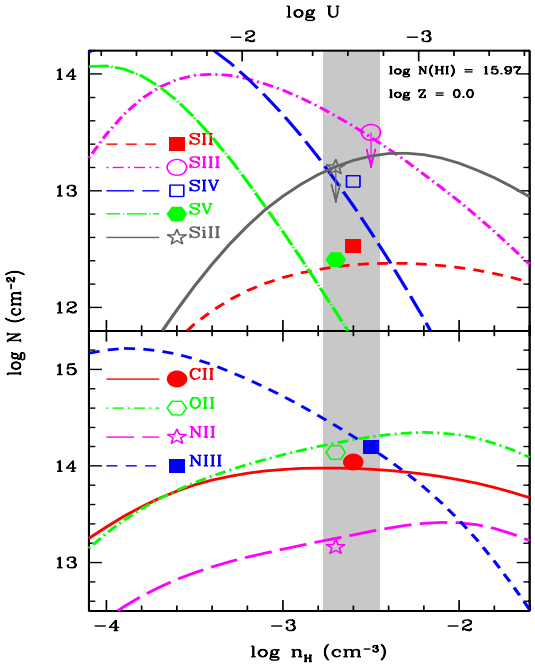

Figure 6. Results of photoionization model for the low-ionization phase. Different curves show the variation of model (with $\log N(\mathrm{H\,I})$ = 15.97 and $Z = Z_{\odot}$) predicted column densities of different low-ions with density. Corresponding ionization parameter is labelled in the top. Measured column densities are indicated by different symbols. The shaded region indicates the density range ($-2.7 \leq \log n_{\mathrm{H}} \leq -2.5$) for which observed column densities are consistent with model predictions.

2004; Spite et al. 2005). However no galaxy candidate is detected close to the QSO line of sight in the SDSS image. Deeper observations of the PG 1407+265 field are needed to arrive at any firm conclusion.

It is apparent from Table 3 that, similar to the other known Ne VIII absorbers, the photoionization model that produces the low ions fails to produce any appreciable column densities for S V, S VI, O VI, and Ne VIII, even with solar metallicity. Therefore it is obvious that these highly ionized species originate from a completely different phase of the absorbing gas. The high ionization phase could be: (a) photoionized with higher ionization parameter than the low ionization gas, (b) collisionally ionized with very high temperature, or (c) in an environment where both photoionization and collisions due to free electrons play an equally important role in deciding the ionization structure and thermal state of the gas.

We find that a density range of $-5.3 \leqslant \log n_{\mathrm{H}} \leqslant -5.0$ (or $-0.2 \leqslant \log U \leqslant 0.1$) is required to reproduce the observed Ne VIII/O VI column density ratios (see bottom panel of Fig. 7). With the help of the ionization simulations, it is fairly straightforward to estimate the line-of-sight thickness for the high ionization phase given the Ne VIII column density:

$$L = \frac{N_{\mathrm{Ne\,VIII}}}{n_{\mathrm{H}} f_{\mathrm{Ne\,VIII}}} \frac{1}{Z} \left(\frac{\mathrm{Ne}}{\mathrm{H}}\right)_{\odot}^{-1}$$
$$\simeq 180 \text{ kpc} \left(\frac{N_{\mathrm{Ne\,VIII}}}{10^{14}}\right) \left(\frac{n_{\mathrm{H}}}{10^{-5}}\right)^{-1} \left(\frac{f_{\mathrm{Ne\,VIII}}}{0.18}\right)^{-1} \left(\frac{1}{Z}\right). \quad (1)$$

Here $f_{\mathrm{Ne\,VIII}} \equiv n_{\mathrm{Ne\,VIII}}/n_{\mathrm{Ne}}$ is the ionization fraction of Ne VIII, which takes a value of 0.18 at $\log n_{\mathrm{H}} = -5.0$, for optically thin conditions. Using Eq. 1, the line-of-sight thickness obtained for the component at -150 km s^{-1} is ∼186 kpc assuming solar metallicity. Such a large size is comparable with the sizes

Table 3. Observed and model predicted column densities

Ion	$\log N$ (cm^{-2}) Observed	$\log N$ (cm^{-2}) Predicted[a]	[X/H]	X
C II	14.04 ± 0.07	13.97	0.07±0.07	C
C III	–	14.92		
C IV	–	13.63		
O II	14.14 ± 0.03	14.27	−0.13±0.03	O
O III	–	15.16		
N II	13.16 ± 0.11	13.28	−0.12±0.11	N
N III	14.20 ± 0.09	14.32		
N IV	–	13.22		
N V	–	11.76		
S II	12.53 ± 0.03	12.36	0.17±0.03	S
S III	< 13.5	13.57		
S IV	13.08 ± 0.15	12.91		
S V	12.41 ± 0.03	11.76		
Si II	< 13.2	13.24	< -0.04	Si
S VI		11.44		
O VI		11.10		
Ne VIII		<10		

Note – [a]Photoionization model predicted column densities for $\log n_{\mathrm{H}} = -2.6$, $\log Z/Z_{\odot} = 0$, and $\log N(\mathrm{H\,I}) = 15.97$.

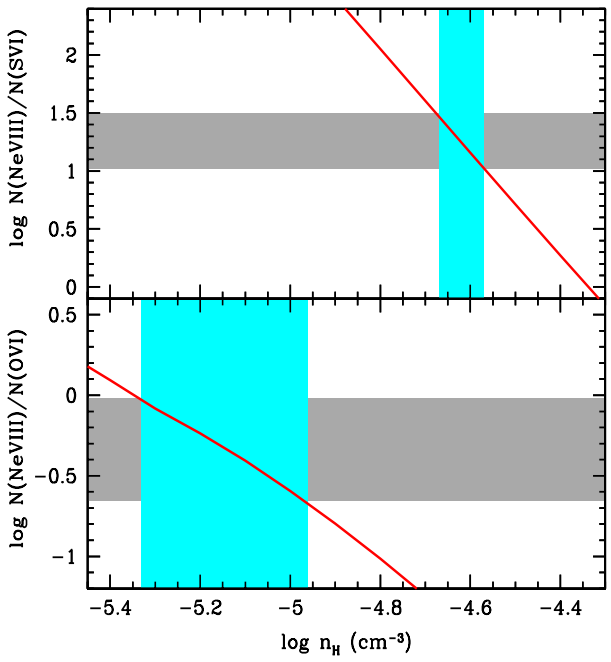

Figure 7. Results of PI model for high ions. Column density ratios Ne VIII/S VI (top) and Ne VIII/O VI (bottom) are plotted against hydrogen number density. The horizontal shaded regions indicate the range of observed column density ratios. The vertical shaded regions (in cyan) correspond to the density range over which a PI model reproduces the observed ratios. Clearly, S VI is severely underproduced for the density range suggested by the Ne VIII/O VI ratio.

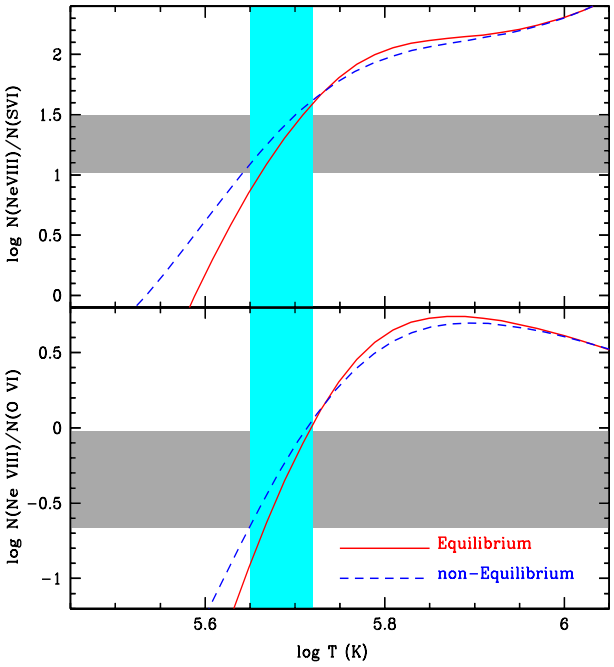

Figure 8. Column density ratios of Ne VIII/S VI (top) and Ne VIII/O VI (bottom) against gas temperature under CIE (solid curve) and non-CIE (dashed curve) models of Gnat & Sternberg (2007). The horizontal shaded region indicates the range in observed column density ratios. The vertical shaded region (in cyan) is the range of temperature for which CIE model successfully reproduces both the ratios. Non-CIE model suggests only slightly wider range in temperature compared to CIE model.

of oxygen-rich halos of isolated star forming galaxies at low redshift ($z < 0.2$, see Tumlinson et al. 2011; Werk et al. 2013, 2014). Evidently, the high ionization gas phase can have a photoionization solution provided the metallicity is high enough (i.e., $Z \sim Z_{\odot}$). Here we argue that the high ionization gas phase cannot have a much lower metallicity (than solar) as we do not see any Lyβ absorption corresponding to the high ion component at ~ -150 km s^{-1} (see Fig. 4)[4]. The total hydrogen column density associated with this high ionization phase is $\log N_{\rm H}({\rm cm}^{-2}) = 19.4$, assuming solar metallicity. This is a factor of 10 more than what we have found for the low ionization phase but is similar to the previously reported values in collisionally ionized Ne VIII absorbers (see e.g. Table 1 of Tepper-García et al. 2013). The H I ionization fraction, $f_{\rm H\,I} = 1.2{\times}10^{-6}$, as computed by CLOUDY, at $\log n_{\rm H} = -5.3$ gives a N(H I) of $10^{13.3}$ cm^{-2} which is consistent with the 3σ upper limit we estimate for the non-detection of Lyβ absorption in the ~ -150 km s^{-1} component. Our photoionization model solutions are summarized in Table 4.

While our two phase photoionization solutions can explain most of the observed ions (low+high), none of the phases can reproduce the right amount of N(S V) and N(S VI). The low ionization phase produces a factor of ∼3 less N(S V) than the observed value. The high ionization phase, on the other hand, produces $\log N < 11$ for both S V and S VI. Fig. 7 clearly shows that the density range for which observed Ne VIII/O VI ratio is well explained by the model fails to produce enough S VI. Such a discrepancy can be sorted out by invoking yet another phase with density in the range $-4.2 < \log n_{\rm H} < -3.5$, where the ionization fractions of S V and S VI show their maxima. Note that such a density range will also produce considerable C IV and N V. These transitions are not covered with the present COS spectrum. Nonetheless, we note that C IV absorption is clearly detected in the low resolution FOS spectra (Jannuzi et al. 1998). N V, on the contrary, is possibly not detected. The measured N(C IV) and upper limit of N(N V) are, indeed, consistent with the above quoted density range. However, because of the low resolution of the FOS spectrum we could not resolve the component structure. Higher resolution data is certainly required for further analysis of the detailed ionization structure. In the next section we investigate if collisional ionization models can successfully explain all the high ions simultaneously in a single phase.

4.2 Collisional ionization model for the high ions

As discussed by Muzahid et al. (2013, see Fig. 21) the N(Ne VIII)/N(O VI) ratios found in intervening systems occupy a narrow range that is occupied by the intrinsic absorbers as well. In addition, they have shown that collisional ionization is indeed a feasible ionization mechanism for the intrinsic Ne VIII absorbers (see also Muzahid et al. 2012b). The observed range in the N(Ne VIII)/N(O VI) ratios in the present system is consistent with the earlier measurements in other intervening systems. In order to understand whether or not the collisional ionization is a viable process for the highly ionized species detected in this system, we consider the models of Gnat & Sternberg (2007). In Fig. 8 we show the variation of Ne VIII to O VI (and S VI) column density ratios against the gas temperature under equilibrium (CIE) and non-equilibrium (non-CIE) isobaric models. The non-equilibrium processes become important for high metallicity ($Z > 0.1Z_{\odot}$) gas. Here we use the isobaric non-CIE model computed at solar metallicity. However, it is apparent from the figure that CIE and non-CIE models give a fairly similar range in temperature (i.e., $5.65 < \log T({\rm K}) < 5.72$) that can explain the observed N(Ne VIII)/N(O VI) and N(Ne VIII)/N(S VI) ratios simultaneously[5]. As expected, this temperature range is consistent with the previous studies of Ne VIII absorbers (e.g., Savage et al. 2005; Narayanan et al. 2011, 2012; Meiring et al. 2013).

As mentioned earlier, we derive a 3σ upper limit on N(H I) $< 10^{13.4}$ cm^{-2} for the high ionization component at ~ -150 km s^{-1}. Using this limit we estimate the metallicity of the collisionally ionized hot gas to be $\log Z/Z_{\odot} > -1.0$ at $T = 10^{5.7}$ K. Although the lower limit on the metallicity is consistent with that of the cool photoionized gas phase, it need not be the case always as it is generally assumed (e.g., Savage et al. 2005; Tripp et al. 2011; Meiring et al. 2013). The total hydrogen column density in this case is $N_{\rm H} < 10^{19.6}$ cm^{-2}. The hot phase CIE solution does not produce any significant amount of N(S V), N(C IV) or any other low/intermediate ions, which indicate the presence of an additional phase.

[4] We obtain a formal 3σ upper limit on N(H I) $< 10^{13.4}$ cm^{-2} using the observed error spectrum.

[5] We note that non-equilibrium isochoric models also give similar temperature range.

Table 4. Summary of photoionization model solutions.

Phase	Species	$\log n_{\rm H}$ ($\rm cm^{-3}$)	$\log U$	$\log Z$ ($Z_\odot$)	$\log N_{\rm H}$ ($\rm cm^{-2}$)	Size	$\log T$ (K)
Low	C II, C III, N II, N III, N IV, O II, O III, Si II, S II, S III, S IV	$-2.6(-2.8)$	$-2.6(-2.8)$	0.0(0.0)	18.5(18.4)	410 pc (480 pc)	3.9 (4.0)
High	O VI, Ne VIII	$-5.3(-5.3)$	$0.1(-0.3)$	0.0(0.0)	19.4(18.8)	186 kpc(175 kpc)	4.8 (4.8)

Note – Values in the parenthesis are for the Haardt & Madau (2012) UV background radiation.

4.3 Hybrid model for the high ionization gas

In order to complete our modelling efforts, we explore a hybrid model in which we consider a hot gas in the presence of the UV ionizing background. This is a more realistic scenario than the pure collisional ionization, as the gas cannot be shielded from the extra-galactic UV background in this non-Lyman limit absorber. The model grids are computed using CLOUDY for an optically thin hot gas at different constant temperatures and exposed to the Haardt & Madau (2001) UV background radiation at $z = 0.6$. With the temperature fixed we try to understand the contribution of photoionization in a hot gas and how that changes with gas temperature. In the top panel of Fig. 9 we show the model predicted Ne VIII/O VI column density ratio against hydrogen density for different (constant) temperature in the range $10^5 - 10^6$ K. Clearly, the observed ratios cannot be reproduced by the hybrid models for $T > 5 \times 10^5$ K. Beyond this temperature collisional ionization dominates over photoionization and $f_{\rm Ne\,VIII}$ increases rapidly towards its peak. Note that this is the best fit temperature implied by pure collisional ionization in Section 4.2. For lower temperatures there are ranges in $n_{\rm H}$ and T that can explain the observed line ratios. Typically, the observed N(Ne VIII) to N(O VI) ratios are well reproduced for density $\log n_{\rm H} < -4.2$ and temperature $T < 4 \times 10^5$ K. Models with $T < 4 \times 10^5$ K can also reproduce the observed N(Ne VIII)/N(S VI), however, at much higher density (see the bottom panel of Fig. 9). Therefore, like photoionization models, a hybrid model also *cannot* reproduce the observed N(S VI), N(O VI), and N(Ne VIII) simultaneously.

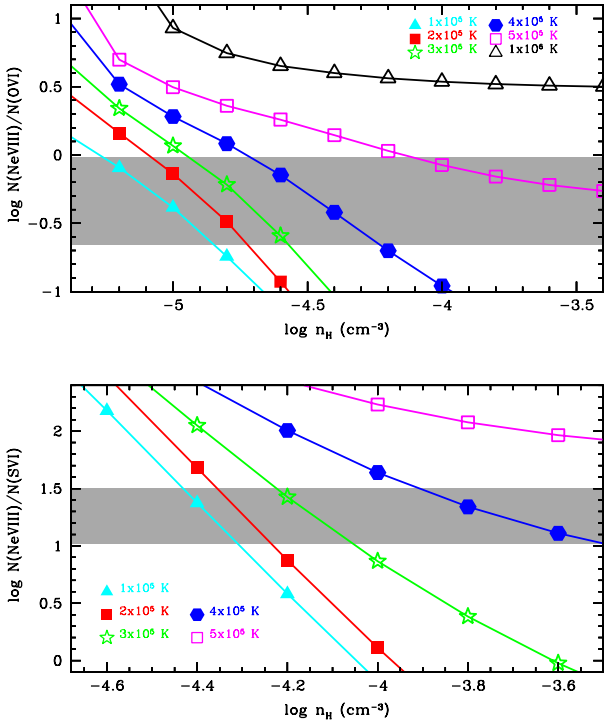

Figure 9. Column density ratios of Ne VIII/S VI (bottom) and Ne VIII/O VI (top) versus the hydrogen density under hybrid (PI+CIE) models. Different curves correspond to different temperatures as indicated in the plot. The horizontal shaded regions show the range in observed ionic ratios.

5 DISCUSSION

5.1 Multiphase Structure

All the low ions detected in this system show a narrow ($\Delta v_{90} \lesssim 90$ km s^{-1}) and single component absorption profiles which are well aligned with the profiles of intermediate ions. Additionally, the line centroid of this component matches with that of the strongest H I component. The intermediate ionization species, however, show an additional weak component separated by -25 km s^{-1}, roughly containing 20% of the observed total column densities of these ions. The absorption profiles of the high ionization species are different compared to that of the low ions. The high ion absorption is comprised of four components spread over $\Delta v_{90} \sim 270$ km s^{-1}. The difference in absorption line kinematics between the high and low ions clearly indicates the multiphase nature of the absorbing gas. Such a disparity between the absorption profiles of high and low ions is in contrast to what has been reported for other Ne VIII system by Tripp et al. (2011) and Meiring et al. (2013).

5.2 Low Ionization Gas

We find that the observed column densities of the low ions and the stronger component of the intermediate ions that are aligned with the strongest H I component can be very well explained by a photoionized gas with a density of $n_{\rm H} = 2.5\times10^{-3}$ cm^{-3} ($\log U = -2.6$) and an absolute metallicity of $Z \sim Z_\odot$ irradiated by the UV background radiation contributed by QSOs and galaxies. The inferred density range in this system is higher than those derived for the similar phase in other known Ne VIII absorbers (see e.g., Table 1 of Tepper-García et al. 2013). The relatively higher hydrogen density with respect to the mean IGM at this redshift (i.e., $\bar{n}_{\rm H} = 7 \times 10^{-7}$ cm^{-3}) suggests that the gas is possibly associated with a very large over-dense region. The total hydrogen column density associated with this cool photoionized phase is $N_{\rm H} = 10^{18.5}$ cm^{-2}. This corresponds to a line-of-sight thickness of $\sim$ 410 pc. The model predicted photoionization equilibrium temperature (i.e., $T \sim 10^{3.9}$ K) is consistent with the observed narrow doppler parameters of H I and metal absorption lines. This cool

photoionized phase is unable to explain the observed line strengths of S V and the high ionization species: S VI, O VI, and Ne VIII.

The relative abundances of C, N, O and S are found to be consistent with the solar values within 0.2 dex. Based on [N/O] and [O/H] ratios we argue that the nitrogen in this system is predominantly synthesized via secondary production mechanism. This indicates that the absorbing gas is in close association with a region with a sustained star-formation for a prolonged period. Such a chemical enrichment is unlike what is seen in high redshift DLAs but resembles the Galactic ISM. This, however, is not surprising as low-redshift systems are expected to have adequate time for secondary production levels to begin. Recently, using a sample of low redshift ($z < 1$) Lyman limit systems (LLS; with $16.2 \leq \log N(\mathrm{H\,I}) \leq 18.5$) Lehner et al. (2013) have found that the metallicity distribution of such absorbers exhibit a bimodal distribution with peaks at $\log Z = -1.6$ and $\log Z = -0.3$ respectively. The authors have claimed that the metal-rich branch likely traces winds, recycled outflows, and tidally stripped gas whereas the metal-poor branch is consistent with cold accretion streams that fuel gas in star forming galaxies. The system under consideration show a total $\log N(\mathrm{H\,I}) = 16.02 \pm 0.03$, which is close to the lower limit of $N(\mathrm{H\,I})$ considered by Lehner et al. (2013). An absolute metallicity of $Z \sim Z_{\odot}$, as we estimate for the low ionization phase, indicates that the system belongs to the metal-rich branch and therefore likely to trace an outflowing material.

The near solar metallicity with solar relative abundances and high [N/O] ratio found here strongly suggest a connection of this absorber to a star-forming region. However, no galaxy candidate at the redshift of the absorber is found in SDSS image. Therefore, this system is not associated with any $L_{\star}$ galaxy, as these will be readily visible with the SDSS images. The apparent magnitude limit of SDSS in the r-band for 95% completeness is $m_{\mathrm{r}} \leqslant 22.2$[6]http://www.sdss3.org/dr10/scope.php/. This magnitude limit corresponds to a limiting luminosity of $L \sim 0.33 L_{\star}$ at the absorber redshift (Montero-Dorta & Prada 2009). Searches for faint galaxies at low impact parameters in deeper images will provide further insights on the absorber that shows signature of being associated to star forming region.

5.3 High Ionization Gas

A low-temperature (i.e., $T < 10^5$ K) optically thin photoionized gas with $n_{\mathrm{H}} < 10^{-5}$ cm^{-3}, exposed to the Haardt & Madau (2001) UV background at $z \sim 0.5$ can have considerable $f_{\mathrm{Ne\,VIII}}$ (e.g., > 0.1) (see Fig. 1 of Tepper-García et al. 2013). Here we show that the observed N(Ne VIII) and N(O VI) can be well reproduced by a gas photoionized by the extragalactic UV-background radiation (Haardt & Madau 2001). The preferred gas density in such a case is $-5.3 \leq \log n_{\mathrm{H}} \leq -5.0$ and the absolute metallicity is close to solar (i.e., $Z \sim Z_{\odot}$). From the absence of Lyβ absorption in one of the high ionization component, we argue that the metallicity of the highly ionized gas is indeed near solar. Estimating the H I content in different phases (high ionization phase, in particular) of a multiphase system is challenging (but see Muzahid 2014, for a special case). However, z_{abs} = 0.59961 towards PG 1407+265 is a unique absorption system where we could constrain the $N(\mathrm{H\,I})$ associated with the high ionization phase directly from data.

In this work, we show that an absorber with N(Ne VIII) = 10^{14} cm^{-2} and with solar metallicity will have a line of sight thickness of $\sim$ 180 to 200 kpc for the density range suggested by the observed N(Ne VIII)/N(O VI) ratio in this system (i.e., $-5.3 \leq \log n_{\mathrm{H}} \leq -5.0$). Such sizes are typical of oxygen-rich halos of low redshift star-forming galaxies (Tumlinson et al. 2011; Werk et al. 2014). In fact, the total O VI column density measured in the system we presented here is $\log N(\mathrm{O\,VI}) = 14.57 \pm 0.05$, which is close to the median value of $N(\mathrm{O\,VI})$ around star-forming galaxies in the sample of Tumlinson et al. (2011). The total hydrogen column density associated with this phase is $N_{\mathrm{H}} \sim 10^{19.4}$ cm^{-2}, which is very similar to those derived for collisionally ionized Ne VIII absorbers (see Table 1 of Tepper-García et al. 2013, for a summary). The photoionization temperature for the high ionization phase is $T \sim 10^{4.8}$ K and is 10 times higher than that of the low ionization phase. The density of high ionization gas, on the other hand, is 500 times lower than the low ionization phase. Therefore it is difficult to sustain a pressure equilibrium between high and low ionization gas (see also the discussion of Muzahid 2014). Nevertheless, photoionization of O VI and Ne VIII is a reasonably good model and we point out that Ne VIII *is not an unambiguous tracer of collisionally ionized hot gas.* The only trouble with this photoionization model is that it cannot reproduce the S VI column density in the same phase. Thus we try to understand these high ions in view of CIE/non-CIE and hybrid models. Nonetheless, we cannot rule out the possibility of yet another photoionized phase with density $-4.2 < \log n_{\mathrm{H}} < -3.5$. The C IV and N V absorption features seen in the low resolution FOS spectra are indeed consistent with such a density range. However, to make any definitive conclusion about this phase it is important to have medium resolution spectrum covering N V and C IV lines.

Under CIE, both Ne VIII/O VI and Ne VIII/S VI column density ratios are well explained with the temperature in the range $5.65 < \log T(\mathrm{K}) < 5.72$. This narrow range in temperature is consistent with previous studies where the temperature is derived from Ne VIII/O VI ratios (e.g., Savage et al. 2005; Narayanan et al. 2011, 2012). Using the 3σ upper limit on $N(\mathrm{H\,I})$ as estimated in one of the high ionization component, we derive a total hydrogen column density, $N_{\mathrm{H}} < 10^{19.6}$ cm^{-2} and metallicity, $Z > 0.1 Z_{\odot}$. This clearly suggests that the metallicity of collisionally ionized warm-hot gas need not be equal to that of cool photoionized phase as it is sometimes assumed (e.g., Tripp et al. 2011; Meiring et al. 2013). Note that the collisionally ionized gas does not produce any considerable amount of $N(\mathrm{S\,V})$. This is in contrast to what have been found by Tripp et al. (2011) for the z_{abs} = 0.927 system towards PG 1206+459 where there was no O VI coverage. Next, we found that a hybrid (PI+CIE) model can explain the observed N(Ne VIII)/N(O VI) ratio for a range of densities and temperatures, but cannot explain observed line strength of S VI in the same phase. Therefore, for the present system, we do not find a compelling case to support the CIE instead of PI models as both of them require similar number of distinct ionization phase.

5.4 Sizes of Ne VIII absorbers

Several previous studies of Ne VIII systems (see e.g., Savage et al. 2005; Narayanan et al. 2011, 2012) have found that the required line-of-sight thickness of the absorber became unreasonably large (i.e., $>$ few Mpc) in order to reproduce the observed N(Ne VIII) via photoionization by the extra-galactic UV background. The Ne VIII system at z_{abs}= 0.20701 towards the QSO HE 0226-4110 analyzed by Savage et al. (2005) has a N(Ne VIII) to N(O VI) ratio very similar to the present system. Assuming $\log Z = -0.5$ and

[6] http://www.sdss3.org/dr10/scope.php/

using old version of the extra-galactic UV background radiation (i.e., Haardt & Madau 1996, "HM96"), the author inferred a line-of-sight thickness of $\sim$ 11 Mpc. The line-of-sight thickness become a factor of 10 less (i.e., $\sim$ 1.3 Mpc) when we use the latest extra-galactic UV background (i.e., Haardt & Madau 2012, "HM12") and $\log Z = -0.5$. Note that the metallicity of this absorber is not well constrained from data but was assumed to be same as measured in the moderately ionized phase. We estimate a line-of-sight thickness of $\sim$ 420 kpc assuming a solar metallicity. The line-of-sight thickness of the $z_{\rm abs}$= 0.32566 system towards the QSO 3C 263 becomes $\sim$ 700 kpc (instead of $\gtrsim$ 1 Mpc as inferred by Narayanan et al. (2012)) when we use "HM12" extra-galactic UV background. Therefore, we conclude that the line-of-sight thickness of the previous Ne VIII absorbers, irradiated with latest UV background radiation ("HM12") get significantly reduced, but still, is very large and hence a photoionized origin can be ruled out.

6 SUMMARY

We present a detailed analysis of a Ne VIII system at$z_{\rm abs}$ = 0.59961 in the high SNR COS spectrum of the QSO PG 1407+265 ($z_{\rm em}$ = 0.94). In addition to Ne VIII, absorption lines from low (C II, N II, O II and S II), intermediate (C III, N III, N IV, O III, S IV and S V), and high (S VI, O VI and Ne VIII) ions are detected at greater than 3σ significance. The Ne VIII λ780 line is detected at a 8σ level with an observed equivalent width of $W_{\rm obs}$ = 52.8$\pm$6.5 mÅ. All these metal ions with significantly different ionization potentials provide stringent constraints on the ionization condition and/or thermal state of the gas. Moreover, several unsaturated higher order H I Lyman series lines (H Iλ937 to λ915) provide an accurate estimate of the neutral hydrogen content and hence of the metallicity of the absorber. We briefly summarize the important results:

1. The velocity profiles of the low (C II, N II, O II and S II) ions are narrow and are perfectly aligned with the intermediate (C III, N III, N IV, O III and S IV) ions. Photoionization model solutions show that the low and intermediate ions origin in a metal enrinched ($Z \sim Z_{\odot}$) over-dense gas of density $n_{\rm H}$ = 2.5$\times10^{-3}$ cm^{-3} having a compact size $\sim$ 410 pc. The density measured in this system is larger than the inferred $n_{\rm H}$ in the low ionization phases of the other known Ne VIII absorbers. The estimated relative abundances of C, N, O and S are consistent with the solar values within 0.2 dex indicating that the photoionized gas was part of a region that sustained star-formation for a prolonged period.

2. The highly ionized species Ne VIII and O VI show a very different spread out velocity profiles compared to the low ions. A diffuse ($\sim$ 180 kpc), low density ($-5.3 \leqslant \log n_{\rm H} \leqslant -5.0$), photoionized gas with solar metallicity can reproduce the observed column densities of Ne VIII and O VI. The above low and high photoionized gas cannot explain the observed column densities of S V, S VI and C IV (detected in the FOS spectrum), which, require an intermediate photoionized gas phase with density $-4.2 < \log n_{\rm H} < -3.5$.

3. A single phase collisional ionization model with $5.65 < \log T < 5.72$ can reproduce the observed column densities of S VI, O VI, and Ne VIII simultaneously. This temperature range is consistent with all the previous Ne VIII absorbers. The metallicity of the collisionally ionized hot gas is $Z > 0.1Z_{\odot}$. This hot phase also fails to reproduce S V and/or C IV column densities which indicate the presence of an intermediate phase. Therefore, whether one uses CIE or PI models, the present system requires at least three distinct phases to reproduce the observed column densities.

4. The line-of-sight thickness of the Ne VIII absorbing gas, irradiated with latest updated extra-galactic UV background radiation Haardt & Madau (2012) is reasonable so the CIE models cannot be favoured simply based on the inferred line-of-sight thickness of the absorbing gas. This is unlike what have been found for all the other known Ne VIII absorbers. Using solar metallicity and latest UV background radiation we checked the sizes of the previously known Ne VIII absorbers under photoionization. The sizes of the absorbers get reduced (compared to the sizes reported using Haardt & Madau (1996) UV background) but still are very large and hence we rule out the possibility of a photoionized origin for these Ne VIII absorbers.

5. The high chemical enrichment of the absorber strongly connects it to a star-forming region. However, no galaxy candidate is detected in the vicinity of the QSO line-of-sight in the SDSS image. Deep search for faint dwarf galaxies with low impact parameters will provide further insights on the absorber-galaxy connections.

7 ACKNOWLEDGEMENT

This work has made use of HST/COS data and therfore we are grateful to all the people associated with the design and construction of COS onboard HST. TH acknowledges IUCAA for travel support, library and computational facilities during the period of this work. AP acknowledges IUCAA visiting associateship program and a DST-SERB grant.

REFERENCES

Cen, R. & Ostriker, J. P., 1999, ApJ, 514, 1
Cooke, R., Pettini, M., Steidel, C. C., Rudie, G. C., & Nissen, P. E., 2011, MNRAS, 417, 1534
Danforth, C. W. & Shull, J. M., 2005, ApJ, 624, 555
—, 2008, ApJ, 679, 194
Danforth, C. W., Shull, J. M., Rosenberg, J. L., & Stocke, J. T., 2006, ApJ, 640, 716
Davé, R., Cen, R., Ostriker, J. P., et al., 2001, ApJ, 552, 473
Dutta, R., Srianand, R., Rahmani, H., Petitjean, P., Noterdaeme, P., & Ledoux, C., 2014, MNRAS, 440, 307
Ferland, G. J., Porter, R. L., van Hoof, P. A. M., et al., 2013, Rev. Mexicana Astron. Astrofis., 49, 137
Fukugita, M. & Peebles, P. J. E., 2004, ApJ, 616, 643
Gnat, O. & Sternberg, A., 2007, ApJS, 168, 213
Green, J. C., Froning, C. S., Osterman, S., et al., 2012, ApJ, 744, 60
Grevesse, N., Asplund, M., Sauval, A. J., & Scott, P., 2010, Ap&SS, 328, 179
Haardt, F. & Madau, P., 1996, ApJ, 461, 20
—, 2001, in Clusters of Galaxies and the High Redshift Universe Observed in X-rays, Neumann, D. M. & Tran, J. T. V., eds.
—, 2012, ApJ, 746, 125
Howk, J. C., Ribaudo, J. S., Lehner, N., Prochaska, J. X., & Chen, H.-W., 2009, MNRAS, 396, 1875
Israelian, G., Ecuvillon, A., Rebolo, R., García-López, R., Bonifacio, P., & Molaro, P., 2004, A&A, 421, 649
Jannuzi, B. T., Bahcall, J. N., Bergeron, J., et al., 1998, ApJS, 118, 1
Kriss, G. A., 2011, Improved Medium Resolution Line Spread Functions for COS FUV Spectra. Tech. rep.
Lehner, N., Howk, J. C., Tripp, T. M., et al., 2013, ApJ, 770, 138

Lehner, N., Savage, B. D., Richter, P., Sembach, K. R., Tripp, T. M., & Wakker, B. P., 2007, ApJ, 658, 680
McDowell, J. C., Canizares, C., Elvis, M., Lawrence, A., Markoff, S., Mathur, S., & Wilkes, B. J., 1995, ApJ, 450, 585
Meiring, J. D., Tripp, T. M., Werk, J. K., Howk, J. C., Jenkins, E. B., Prochaska, J. X., Lehner, N., & Sembach, K. R., 2013, ApJ, 767, 49
Montero-Dorta, A. D. & Prada, F., 2009, MNRAS, 399, 1106
Muzahid, S., 2014, ApJ, 784, 5
Muzahid, S., Srianand, R., Arav, N., Savage, B. D., & Narayanan, A., 2013, MNRAS, 431, 2885
Muzahid, S., Srianand, R., Bergeron, J., & Petitjean, P., 2012a, MNRAS, 421, 446
Muzahid, S., Srianand, R., Savage, B. D., Narayanan, A., Mohan, V., & Dewangan, G. C., 2012b, MNRAS, 424, L59
Narayanan, A., Savage, B. D., & Wakker, B. P., 2012, ApJ, 752, 65
Narayanan, A., Savage, B. D., Wakker, B. P., et al., 2011, ApJ, 730, 15
Narayanan, A., Wakker, B. P., & Savage, B. D., 2009, ApJ, 703, 74
Osterman, S., Green, J., Froning, C., et al., 2011, Ap&SS, 335, 257
Penton, S. V., Stocke, J. T., & Shull, J. M., 2004, ApJS, 152, 29
Persic, M. & Salucci, P., 1992, MNRAS, 258, 14P
Petitjean, P., Ledoux, C., & Srianand, R., 2008, A&A, 480, 349
Richter, P., Savage, B. D., Sembach, K. R., & Tripp, T. M., 2006, A&A, 445, 827
Richter, P., Savage, B. D., Tripp, T. M., & Sembach, K. R., 2004, ApJS, 153, 165
Savage, B. D., Kim, T.-S., Wakker, B. P., Keeney, B., Shull, J. M., Stocke, J. T., & Green, J. C., 2014, ApJS, 212, 8
Savage, B. D., Lehner, N., Wakker, B. P., Sembach, K. R., & Tripp, T. M., 2005, ApJ, 626, 776
Savage, B. D., Narayanan, A., Lehner, N., & Wakker, B. P., 2011, ApJ, 731, 14
Savage, B. D. & Sembach, K. R., 1991, ApJ, 379, 245
Savage, B. D., Sembach, K. R., Tripp, T. M., & Richter, P., 2002, ApJ, 564, 631
Sembach, K. R., Tripp, T. M., Savage, B. D., & Richter, P., 2004, ApJS, 155, 351
Spite, M., Cayrel, R., Plez, B., et al., 2005, A&A, 430, 655
Sutherland, R. S. & Dopita, M. A., 1993, ApJS, 88, 253
Tepper-García, T., Richter, P., & Schaye, J., 2013, MNRAS, 436, 2063
Thom, C. & Chen, H.-W., 2008, ApJS, 179, 37
Tripp, T. M., Giroux, M. L., Stocke, J. T., Tumlinson, J., & Oegerle, W. R., 2001, ApJ, 563, 724
Tripp, T. M., Meiring, J. D., Prochaska, J. X., et al., 2011, Science, 334, 952
Tripp, T. M., Savage, B. D., & Jenkins, E. B., 2000, ApJ, 534, L1
Tripp, T. M., Sembach, K. R., Bowen, D. V., Savage, B. D., Jenkins, E. B., Lehner, N., & Richter, P., 2008, ApJS, 177, 39
Tumlinson, J., Werk, J. K., Thom, C., et al., 2011, ApJ, 733, 111
Werk, J. K., Prochaska, J. X., Thom, C., Tumlinson, J., Tripp, T. M., O'Meara, J. M., & Peeples, M. S., 2013, ApJS, 204, 17
Werk, J. K., Prochaska, J. X., Tumlinson, J., et al., 2014, ArXiv e-prints